Electrophysiological analysis of HEK293 and RBL cells via patch clamp

Stephan Drothler

I. INTRODUCTION

Patch-clamp describes a biophysical method that allows the electrophysiological study of cells. It enables precise measurements of ion currents fluctuating through single channels or entire cells. A glass micropipette pre-filled with a defined electrolyte solution and attached to the cell membrane by approaching it first with a micromanipulator, followed by a suction induced underpressure that seals the cell membrane to the pipette. This seak is characterized by a high electrical resistance in the giga-Ω range and therefore called gigaseal. To enable electrical detection a electrode is placed into the pipette beforehand, as well as a reference electrode into the extracellular solution. Ion flow in the cell can now be measured with various techniques. Patch-clamp allows the measurement of single ion channels in the cell-attached mode, as well as the measurement of the current through all ion channels in the cell membrane via the whole-cell mode. The inside-out and outside-out recordings allow the possibility to control the composition of the extracellular solution on both sides of the membrane patch. The two approaches used in this experiment, are cell-attached, which can be achieved with the traditional gigaseal and whole cell, where additional sucction after the gigaseal formation enable intracellular current detection through membrane rupture (Romanin 2019b).

Ion channels fulfill various essential tasks in cells, ranging from homeostatis to excitability and cell signaling. Human mutations of various Ca^{2+} proteins have been linked to diseases. These mutations impair specific components of the Ca^{2+}-machinery and consequently leads to the disruption of Ca^{2+} homeostasis (Bagur and Hajnóczky 2017). Also in immune responses the relevance of ion channels in various immune cells is studied. Rapid mast cell degranulation has been traced to their membrane potential changes. This process can cause allergic rhinits or anaphylaxis in allergic persons. Therefore ion channels are a major interest for biomedical research, e.g. the K^+ of mast cell can be depolarized and thereby inactivated (Romanin 2019a).

First a single K^+-channel measurement of rat basophilic leukemia cells is performed and second a whole cell experiment of human embryonic kindney cells, transfected with a voltage-gated Ca^{2+}-channel is conducted.

II. METHODS AND MATERIALS

A. MATERIALS

1) Tools:

- pipette pull machine
- micromanipulator setup
- syringe

2) Chemicals & Organisms:

- Rat basophilic leukemia (RBL) cells
- Pipette solution (P1) (pH 7.4, 145 mM KCl 10 mM D-Glucose 10 mM HEPES 1 mM $MgCl_2$)
- Extracellular solution (E1) (pH 7.4 140 mM NaCl 5 mM KCl 5 mM $MgCl_2$ 10 mM HEPES 10 mM D-Glucose 2 mM $CaCl_2$)
- Human embryonic kidney 293 (HEK293) cells transfected: α1C, β2a and $\alpha 2\delta$
- Pipette solution (P2) (pH 7,2 - 7,4 145 mM Cs methane sulphonate 8 mM NaCl 3.5 mM $MgCl_2$)
- Extracellular solution (E2) (pH 7,2 - 7,4 145 mM NaCl 5 mM CsCl 1 mM $MgCl_2$ 4 mM Mg-ATP 10 mM HEPES 10 mM EGTA 10 mM HEPES 10 mM Glucose 10 mM $CaCl_2$)

B. METHODS

1) K^+-CHANNEL MEASUREMENT IN RBL CELLS:

A series of voltages from -20 to +80 mV were applied in steps of 10 mV to observe the opening and closing of single inward rectifying K^+ ion channels. The voltages were applied for 10 second-intervals with 2 second-interval breaks between them. The K^+ concentration of the solution in the micropipette was prepared to be equivalent to the intracellular concentration, which means, that the only driving force for ion flux was the applied electrical gradient. After recording in the cell-attached mode, the configuration was switched to the whole-cell mode to determine the current over applied voltage relationship.

$$I_{\text{total}} = I_{\text{SC}} \times p \times N \tag{1}$$

This allows the determination of the total current (I_{total}). The resting potential of the cell was estimated graphically while the total amount of channels (N) was calculated from I_{total}, the current through a single channel (I_{SC}) and the open probability of a single channel (p) (Eq. 1).

2) Ca^{2+}-CHANNEL MEASUREMENT IN HEK293:

HEK293 cells were transfected with α1C, β2a and $\alpha 2\delta$ prior to the experiment. These are the subunits forming the voltage-dependend L-type CaV1.2 channel, which is studied in this experiment (Romanin 2019a). A microscope coverslip that was seeded with the HEK cells was washed three times with intracellular solution (0mM Ca^{2+}) to remove the culture medium, put into a cell chamber, covered with extracellular solution (10mM Ca^{2+}) and placed into the micromanipulator setup. The steady-state activation was measured with a holding potential of -70 mV and depolarizations to voltages between -40mV to -90mV in steps of 10mV. The obtained

data was used to calculate the current-voltage relationship of the channels as well as the maximum conductance, fractional conductance (= steady-state activation) and the reversal potential. L-type CaV1.2 VGCCs tend to inactivate upon depolarization. The steady-state inactivation was performed with a holding potential to -70mV and the depolarization-steps where done in the range from -100mV to 0mV with a duration of 5 seconds. The depolarization was set to a maximum channel activation of 400 ms for the investigation of the amount of inactivated channels. This data was used to calculate the steady-state inactivation for the applied potentials as well as the fractional conductance and steady-state activation. The window current was determined, which visualizes the amount of activated channels that remain open.

III. RESULTS

A. K^+-CHANNEL MEASUREMENT IN RBL CELLS

The observation software linked to the micromanipulator was used to screenshot the plots and re-transform via imageJ was performed (Schneider, Rasband, and Eliceiri 2012). The data processing was performed via R studio (V 1.2.1335) and visualized via the ggplot2 package (R Core Team 2019, Wickham 2016).

Voltage [mV]	$Current_{Single}$[mV]	open time [s]	open probability (p)
-20	0,89	1,02	0,1017
-10	1,40	1,97	0,1974
0	2	1,66	0,1664
10	2,41	1,39	0,1389
20	2,93	0,66	0,0657
30	3,51	0,47	0,0466
40	4,20	0,65	0,0654
50	4,88	0,56	0,0562
60	5,49	0,22	0,022
70	6,38	0,30	0,0296
80	7,07	0,29	0,0289

TABLE I: Measured values from the single channel traces, via imageJ. p is calculated from the $\frac{opentime}{recordedtime}$ ratio, with a recorded time of 10 s.

Voltage [mV]	U_{eff} [mV]	$Current_{Whole}$[pA]	Number of Channels (N)
-20	-10.73		
-10	-20.73		
0	-30.73		
10	-40.73		
20	-50.73		
30	-60.73		
40	-70.73		
50	-80.73		
60	-90.73	21	175,27
70	-100.73	58	308,10
80	-110.73	119	581,21

TABLE II: Calculation of U_{eff} via $U_{eff} = U_{rest} - U_{applied}$, serves for the respective $Current_{whole}(I_{total})$ determinations, demonstrated in Fig. 1b. The Figure also illustrates the determination of the reversal potential of -84,79 mV. U_{eff} hast to be bigger than the reversal potential and the calculation of N is performed via Equation 1, which consequently explains the lacking data in I_{total} and N column from -20:50 mV.

Figure 1a is generated from the data in Table I and illustrates the current-voltage correlation of a single K^+-channel fitted with a linear regression. R^2 indicates a good linear fit, moreover the regression equation enables the calculation of

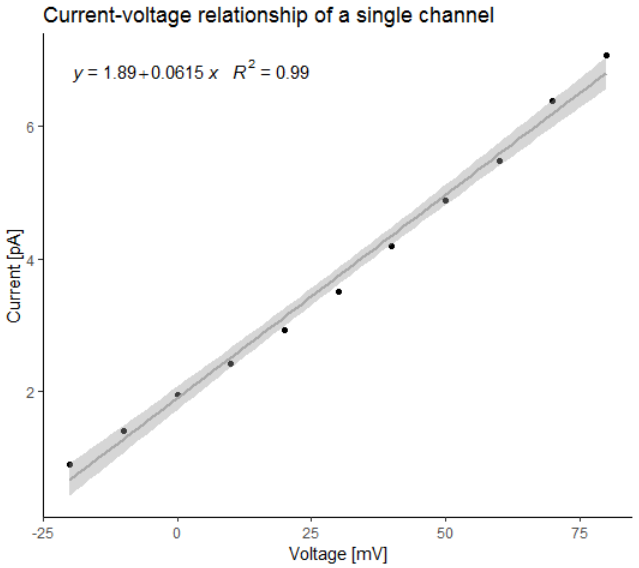

(a) Linear regression line for the Current/Voltage values derived from Table I. Setting y = 0 yields the U_{rest} of -30,73 mV while the slope outlines the the single channel conductance of σ = 0,0615 pS.

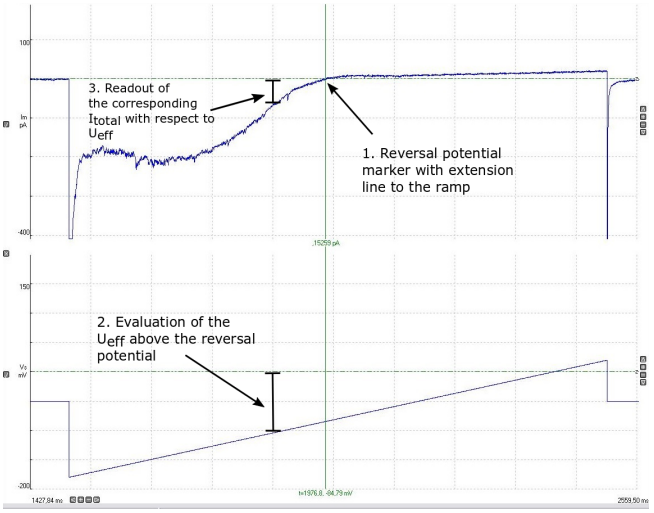

(b) Stepwise demonstration for obtaining I_{total} for individual U_{eff}. The green line described in step one, marks the reversal potential, where ion flux is reversed. This sets the area for U_{eff}, which mappes the respective values to the corresponding I_{total}.

Fig. 1: The current-voltage plot leads to the determination of U_{rest}, thereby to the calculation of U_{eff} which ultimately leads to the generation of the total number of ion channels in the measured cell.

U_{rest} of -30,73 mV. The slope of the regression represents the single channel conductance of σ = 0,0615 pS. Table II leads to an average of $\approx$ 355 channels in the measured RBL cell.

B. Ca^{2+}-CHANNEL MEASUREMENT IN HEK293

The fractional conductance (f_c) is calculated from the data in Figure 2 via Equation 2 and displayed in Table III. Input of σ_{max} = 5,27 pS and U_{rev} = 74 mV.

$$f_c = \frac{I_{applied}}{\sigma \times (U_{applied} - U_{rev})} \quad (2)$$

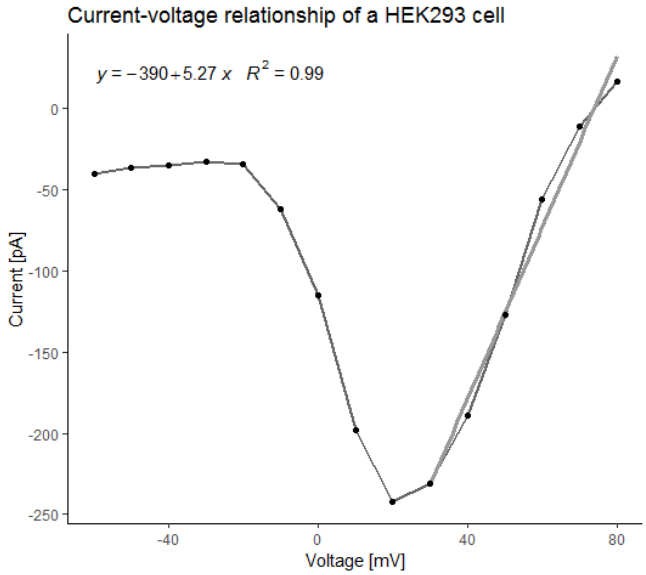

Fig. 2: Linear regression line for the Current/Voltage values derived from Table III. Setting y = 0 yields the reversal potential U_{rev} of 74 mV while the slope outlines the max single channel conductance of σ_{max} = 5,27 pS.

$Current_{Whole}$[mV]	Voltage [mV]	Fractional conductance
-40,167	-60	0,056879266
-35,983	-50	0,055063659
-35,156	-40	0,058517261
-32,647	-30	0,059566122
-34,32	-20	0,069280149
-61,947	-10	0,139936297
-114,644	0	0,29397405
-198,333	10	0,588036646
-241,893	20	0,85
-231,18	30	0,996981197
-189,138	40	1,055575399
-127,196	50	1,005660974
-56,067	60	0,759921388
-10,911	70	0,51759962
16,757	80	0,529949399

TABLE III: Listing of data from the current-voltage relationship and calculated values for f_c (Fig. 2).

$Current_{Whole}$[mV]	Voltage [mV]	Normalized $Current_{Whole}$
-204,25	-70	1
-200,99	-65	0,984024714
-188,73	-60	0,923976637
-185,30	-55	0,907183738
-184,31	-50	0,902380871
-175,98	-45	0,861583428
-172,06	-40	0,842381752
-168,14	-35	0,823184972
-159,80	-30	0,782382633
-145,11	-25	0,710427754
-128,43	-20	0,62878391
-94,36	-15	0,461990766
-58,82	-10	0,28799577
-44,61	-5	0,218395813
-24,20	0	0,118480512
-15,20	5	0,074437095
-8,34	10	0,040817026
-5,56	15	0,027211351
1,49	20	-0,00729977
8,83	25	-0,043230699

TABLE IV: Steady state inactivation data with calculated normalized Current: $\frac{I}{I_{max}}$.

Subsequently f_c is plotted and displays the steady-state activation of the cell (Fig. 3a). The steady state inactivation

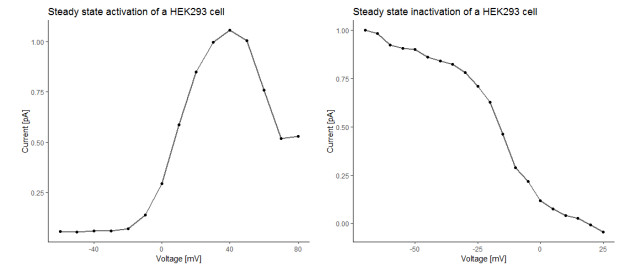

(a) Steady-state activation of Ca^{2+}-channels via fractional conductance (Tab. III).

(b) Steady state inactivation of Ca^{2+}-channels via the normalized current (Tab. IV).

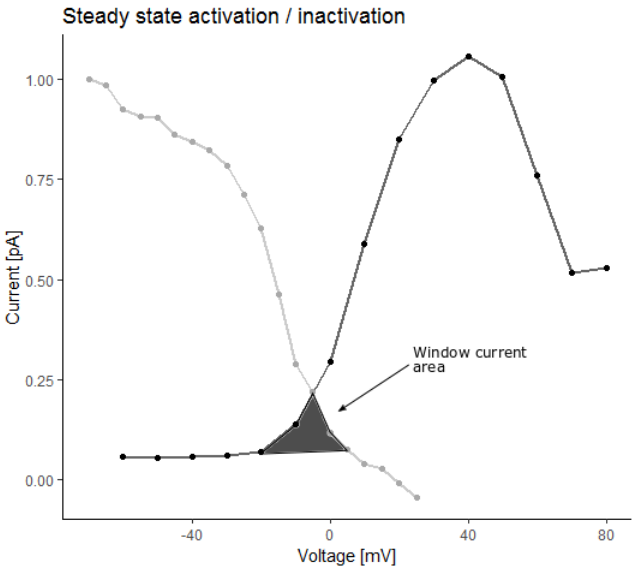

(c) Overlay of the steady-state activation and inactivation plots in order to graphically present the window current area. The peak of the window current is ≈ -2 mV. The activation plot was estimated to be sigmoid, while the inactivation was assumed to be linear for the part of interest.

Fig. 3: Representation of the activation and inactivation curves with subsequent overlay of the two curves.

is plotted on Figure 3b(Tab. IV) with and overlayed with the fractional conductance plot in Figure 3c. The window current is $\frac{124}{100} + \frac{73.5}{100}$ according to an estimated integration of:

$$\int_{-20}^{-2} = \frac{0.5}{1+e^{-0.2\cdot(x)}}\ dx\ + \int_{-2}^{5} = -0.03x\ + 0.15\ dx \quad (3)$$

The formulas of the plots are only rough estimates for the respective part of interest. Both curves appear to be sigmoid, while the inactivation curve was simply assumed to be linear in the segment.

IV. DISCUSSION

The data from the first experiment with the RBL cells yielded 355 total channels and U_{rest} of only -30,73 mV. This is in strong contrast to the literature value of -90 mV (Lindau and Fernandez 1986). The mathematical correlation (R^2 = 0,99) and graphical representations follow the expected sheme, which indicates a correct excecution of the experiment. The strong deviation might be due to the fact that the cell might have been unsuitable because of possible intra-

or extracellular factors like age, size or stress. Consequently the total number of channels should be ≈300 % higher (3× U_{rest}) of N ≈ 1065.

The activation and inactivation curves display the probability densities of open activated state or closed inactivated state channels. Within the window, the inactivation curve indicates that the majority of Ca^{2+} channels are inactivated. The overlapping activation curve that forms the window means that there is a probability that any noninactivated, resting Ca^{2+} channel may open spontaneously at these voltages (Frenz et al. 2014). The window peaks at ≈ 2 mV and represents an area of 0,9875 % ($\frac{197.5}{200}$) of the total activation-inactivation area. The curves roughly follow the expected sheme of sigmoid and inverted sigmoid functions and the correlation of the current-voltage plot (R^2 = 0,99) is also high. Unfortunately there was no literature for the neither the window current determination nor the integration of values. The Paper from C.T. Frenz didn't integrate the area of the window current and thereby irritates the necessity of this calculation.

The data acquisition in both experiments was relatively inaccurate due to the transformation of the values via the Software ImageJ. Raw data files would have provided a more consistent and precise basis for further calculations.

V. APPENDIX

The experiments were performed at Gruberstrae 40, Linz, Austria on 13.05.19 and 15.05.16 under the supervision of Herwig Grabmayr and Adéla Křížová. The experiments were carried out by Caroline Rieser, Lukas Schartel and Stephan Drothler.

REFERENCES

[BH17] Rafaela Bagur and György Hajnóczky. "Intracellular Ca2+ sensing: its role in calcium homeostasis and signaling". In: *Molecular cell* 66.6 (2017), pp. 780–788.

[Fre+14] Christopher T Frenz et al. "NaV1. 5 sodium channel window currents contribute to spontaneous firing in olfactory sensory neurons". In: *Journal of neurophysiology* 112.5 (2014), pp. 1091–1104.

[LF86] MANFRED Lindau and Julio M Fernandez. "A patch-clamp study of histamine-secreting cells." In: *The Journal of general physiology* 88.3 (1986), pp. 349–368.

[R C19] R Core Team. *R: A Language and Environment for Statistical Computing*. R Foundation for Statistical Computing. Vienna, Austria, 2019. URL: https://www.R-project.org/.

[Rom19a] Univ.Pro.Dr. Christoph Romanin. "Patch clamp-Whole cell Recording". 2019.

[Rom19b] Univ.Pro.Dr. Christoph Romanin. "The patch-clamp technique single channel recording". 2019.

[SRE12] Caroline A Schneider, Wayne S Rasband, and Kevin W Eliceiri. "NIH Image to ImageJ: 25 years of image analysis". In: *Nature methods* 9.7 (2012), p. 671.

[Wic16] Hadley Wickham. *ggplot2: Elegant Graphics for Data Analysis*. Springer-Verlag New York, 2016. ISBN: 978-3-319-24277-4. URL: https://ggplot2.tidyverse.org.